Dewetting behaviour of liquid bridges stretched by an accelerated plate

Sebastian Brulin*, Ilia V. Roisman, Cameron Tropea
Institute of Fluid Mechanics and Aerodynamics, Technische Universität Darmstadt,
Darmstadt, Germany

Abstract

Liquid bridge stretching is of interest for a wide field of industrial applications like printing and coating, but also for the functioning of aircraft engines because of its importance in the process of ice crystal icing. In the present experimental study, the focus lies on describing the geometry of the liquid bridge during the stretching process with respect to midpoint diameter, contact line diameter and contact angle for constant accelerations from $10\,\mathrm{m/s^2}$ up to $180\,\mathrm{m/s^2}$. The observed evolution of the dynamic contact angle is described as a function of the capillary number. For the early phase of the stretching process relations for the curvature and midpoint diameter are proposed.

Introduction

Liquid jets have been studied for hundreds of years, and despite the existing understanding of the break-up mechanisms of jets, drops and sheets [2,3] some fundamental questions about the bridge geometry leading to bridge break-up still need to be addressed. Better understanding of the liquid bridge break-up behaviour, especially under dynamic conditions, is significant for industrial applications like printing and coating, but also for the functioning of aircraft engines because of the occurrence of ice crystal icing involving liquid bridges

The time scale for the break-up instant, which was derived and experimentally validated for high stretching rates [1], is determined by surface tension, viscosity and initial bridge geometry. No effect of wettability on the time scale appeared to be involved, whereas the dynamics of moving contact lines and contact angle hysteresis were identified as important parameters during the stretching process by [4–6].

In the present work, the dynamics of a stretching liquid bridge between two solid substrates, one of which moves with a constant acceleration, is studied. Experiments on fast bridge stretching are performed with the aim to better understand the wettability effects and their effect on the liquid bridge break-up. The focus lies on describing the geometry evolution close to and far from the wetting region for small and larger initial bridge heights and for low and high viscous liquids. The maximum bridge height is determined by a constant curvature shape and with no visible gravitational influence on the initial bridge contour ($Bo < 1$). This study tries to find transition conditions at which the influence of the wettability on the stretching process becomes dominant. The measurements involve different non-dimensional initial gap heights, i.e. initial bridge height, initial bridge radius, for a wide range of accelerations. These values are particularly relevant for the application associated with ice crystal icing. Deionized water and water-glycerol mixtures are used to vary the viscosity, surface tension and contact angle.

Experimental Methods

Experimental Setup

The experimental setup shown in figure 1 consists of three main systems: the *stretching apparatus*, the *observation system* and the *fluid dispensing system*. The *stretching apparatus* has two parallel solid substrates and a linear drive system. The upper substrate remains fixed while the lower one is connected to the linear drive and moves with constant acceleration from 10 to $180\,\mathrm{m/s^2}$. The positioning accuracy of the linear drive is $5\,\mu\mathrm{m}$ while the speed is adjustable from $10\,\mathrm{mm/s}$ up to $5\,\mathrm{m/s}$. Both solid substrates have identical surfaces made out of polished aluminium ($R_a = 2.7\,\mu\mathrm{m}$). The *observation system* consists of a high-speed video camera with a telecentric lens and a telecentric illumination. The recording frame rate is set to $12\,000\,\mathrm{fps}$ with a resolution of $512\,\mathrm{px} \times 1024\,\mathrm{px}$. The shutter time stays fixed at $1/25\,000\,\mathrm{s}$. For the *fluid dispensing system*, a microlitre syringe is used. The measurements are performed with the liquid volumes 3, 5 and 7 µl. The measured liquid properties viscosity and surface tension can be found in table 1.

From the recorded videos, an in-house post-processing script identifies the instant of the bridge break-up, the bridge midpoint diameter, the contact lines at the top and bottom, the contact angles and the filament length directly after the bridge break-up.

*Corresponding author: brulin@sla.tu-darmstadt.de

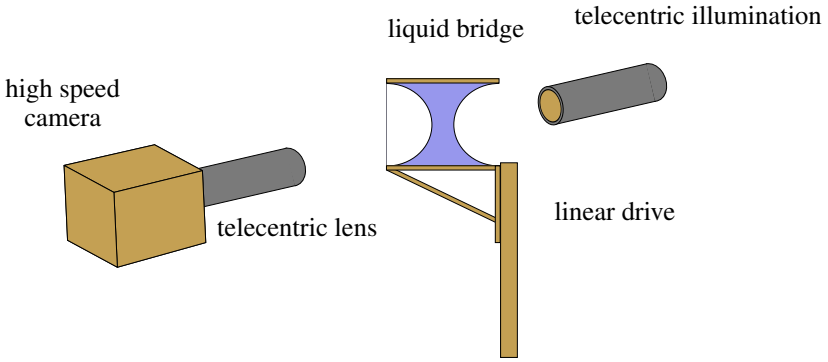

Figure 1. Experimental Setup.

Table 1. Liquid Properties

Abbreviation	Liquid	μ, $\mathrm{kg\,m^{-1}s^{-1}}$	σ, $\mathrm{N\,m^{-1}}$	ρ, $\mathrm{kg\,m^{-3}}$
DW	deionised water	9×10^{-4}	71.8×10^{-3}	997
Gly10	90/10 m-% water-glycerol	1.1×10^{-3}	71.1×10^{-3}	1023
Gly40	60/40 m-% water-glycerol	3.59×10^{-2}	69.1×10^{-3}	1040
Gly80	20/80 m-% water-glycerol	4.13×10^{-2}	65.5×10^{-3}	1211

Observations The experimental setup allows shadowgraph images of the liquid bridge to be taken during the dynamic stretching process. A sample measurement series of $5\,\mu\mathrm{l}$ deionised water with plate accelerations of 10, 90 and $180\,\mathrm{m/s^2}$ is shown in figure 2. The liquid bridge deformation for low accelerations $10\,\mathrm{m/s^2}$ is visible in the image sequence in a): the bridge contour stretches vertically and constricts horizontally. The necking behaviour of the bridge continues until bridge break-up sets in and a small thread forms between the remaining volumes residing on the two substrates. Comparing the different image sequences from figure 2, it is obvious that with increasing acceleration the liquid bridge is stretched for a longer distance before the first break-up occurs. After the break-up from both the upper and lower substrates, a liquid filament is formed between the two residual liquid drops. The height and width of the filament grows with increasing substrate acceleration.

Another occurrence in the higher acceleration sequence is the asymmetric deformation of the ligament heads. While the instants for the upper and lower break-up are nearly identical for $10\,\mathrm{m/s^2}$, they deviate in time from each other with increasing acceleration. This results in a longer deformation phase on one side of the liquid bridge and, after the first break-up, in an asymmetric shape of the ligament. Shortly after the detachment of the ligament, the filament length reduces due to the formation of spheres at the end and a vertical contracting motion of the entire filament. The beginning of sphere formation is similar to rim formation at the edge of a liquid sheet [2], [1]. For long ligaments the cylindrical filament disintegrates into further spheres as shown in figure 2 f), according to the Plateau-Rayleigh instability [7]. Experiments with the same boundary conditions for a glycerol-water mixture are shown in figure 2 a), b) and c). Compared to the experiments in figure 2 d), e) and f) the liquid bridge height for similar accelerations becomes larger before the break-up starts. Therefore, the initial ligament length also increases. The speed of contraction and sphere formation are slower compared to those in figure 2 d), e) and f).

Figure 3 represents the midpoint diameter evolution of the ligament until break-up for different viscosities μ, accelerations a and dimensionless heights $k = H_0/R_0$. The dimensionless height k is a geometric parameter depending on the initial liquid bridge height H_0 and the initial midpoint diameter R_0. Within the investigated viscosity range ($1\,\mathrm{mPa} < \mu < 40\,\mathrm{mPa}$) the influence of viscosity on the midpoint diameter apperas to be negligible and the evolution of the midpoint diameter can be considered as equal. For lower accelerations the evolution of the midpoint diameter becomes flatter and this can also be observed for smaller non-dimensional heights k in figure 4.

The influence of the dimensionless height on the contact line diameter evolution is shown for the accelerations

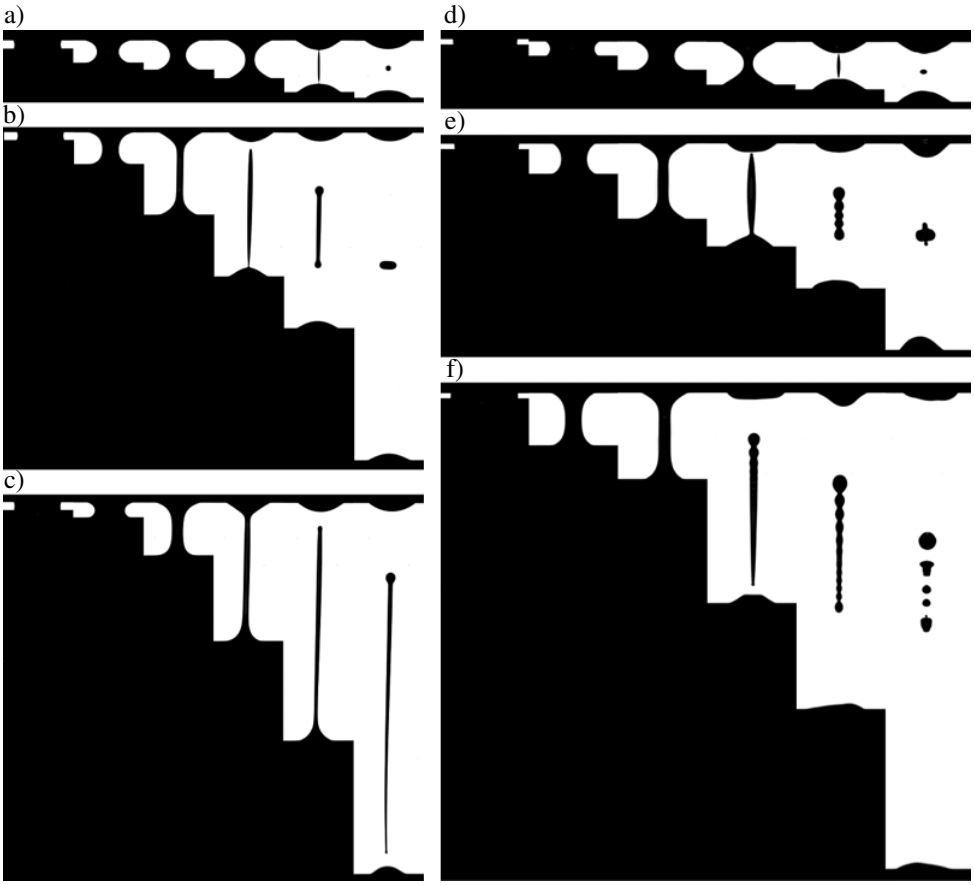

Figure 2. Stretching of liquid bridges consisting of 5 µl glycerol-water mixture for a) $10\,\mathrm{m/s^2}$, b) $90\,\mathrm{m/s^2}$ and c) $180\,\mathrm{m/s^2}$ plate accelerations on the left side and for deionized water for d) $10\,\mathrm{m/s^2}$, e) $90\,\mathrm{m/s^2}$ and f) $180\,\mathrm{m/s^2}$ plate accelerations on the right side.

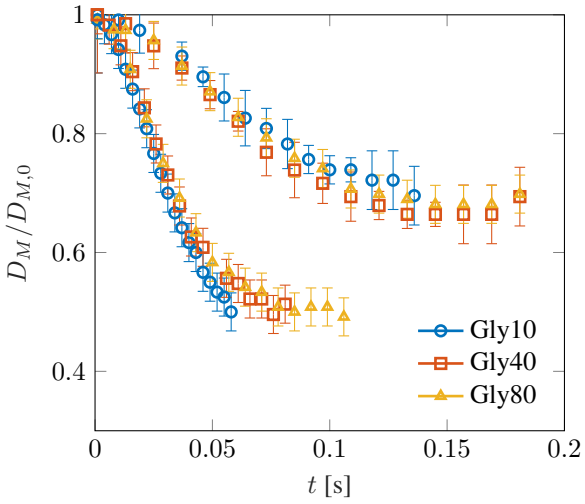

Figure 3. Evolution of the midpoint diameter comparing different viscosities and $k = 0.09$ with an acceleration $180\,\mathrm{m/s^2}$ in the lower curve array and for $10\,\mathrm{m/s^2}$ in the upper curve array.

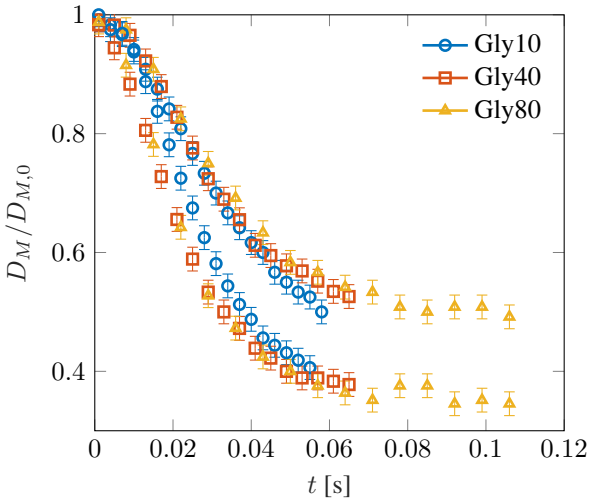

Figure 4. Evolution of the midpoint diameter comparing non-dimensional initial bridge geometries $k = 0.3$ in the lower curve array and for $k = 0.09$ in the upper curve array for substrate accelerations $180\,\mathrm{m/s^2}$ and different viscosities.

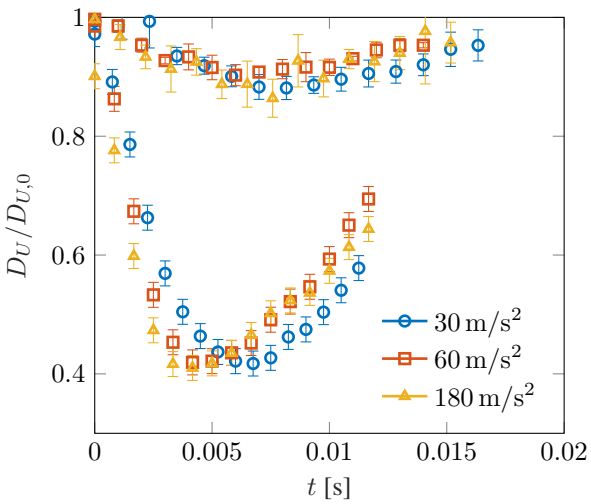

Figure 5. Evolution of contact line diameter of Gly80 comparing substrate accelerations 30 , 60 and for 180 m/s^2 for $k = 0.3$ in the upper curve array and $k = 0.09$ in the lower curve array.

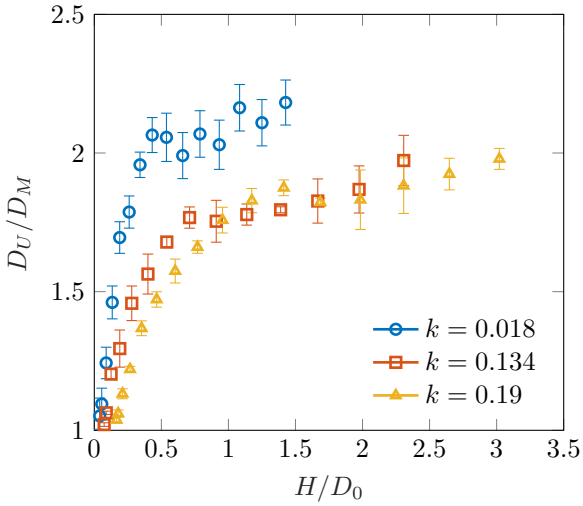

Figure 6. Evolution of the contact line diameter to midpoint diameter ratio up to break-up of the liquid bridge. The measurements were performed with Gly80 and 180 m/s^2 for different k values.

30 , 60 and 180 m/s^2 and two dimensionless heights $k = 0.3$ and $k = 0.09$ in figure 5. The evolution of the ratio $D_U/D_{U,0}$ shows simultaneous movement of the contact line as soon as the lower substrate begins its downward motion ($t = 0$ ms). It is apparent from figure 5 that the ratio $D_U/D_{U,0}$ decreases faster for smaller values of k. Due to the increased speed of the contact line diameter, $D_{U,\min}/D_{U,0}$ exhibits an overall decline by 50% only through smaller k values. The measurements with different accelerations but constant k differ little, due to the different slope magnitudes at the beginning. The $D_{U,\min}/D_{U,0}$ ratio is independent of the plate acceleration. The parameter viscosity shows similar effects on $D_U/D_{U,0}$ as shown for the midpoint diameter in figure 3.

The moving contact line is described with the help of the constant volume condition, comparing the initial geometry parameters $D_{U,0}$ and H_0 with their evolving values. The error made by assuming a cylindrical liquid bridge can be derived from figure 6. Due to the compressing of the liquid after applying the sample liquid on the substrate, the initial contact angle is relatively large. Therefore, the bridge has a columnar shape and an initial ratio of $D_U/D_M \approx 1$. With further stretching the values of D_U and D_M deviate up to a ratio $D_U/D_M \approx 2.1$ for the smallest investigated bridges. The effect of the initial bridge geometry is a steeper inclination for smaller bridges and an increasing diameter ratio at break-up.

Results and Discussion

In order to obtain a better understanding of the evolution of the contact line diameter movement $D_U/D_{U,0}$, the contact angle θ is examined in figure 7. For smaller liquid bridges shown in figure 8 the contact line diameter contraction is larger compared to the one shown in figure 7. It is apparent in both cases that the contact angle decreases to a minimum value of approximately 20°. After reaching $\theta_{\min}$ the contact angle starts to increase again as for $D_U/D_{U,0}$. But the contact angle growth starts earlier than the contact line diameter contraction.

At the beginning of the stretching process, a constant radius of curvature can be observed over the height of the liquid bridge on both sides. The measured radius of curvatures for different accelerations are shown in figure 10. The dispensed fluid initially shows a high contact angle state due to the compression, as discussed in the previous section. This results in small radius of curvatures at the beginning. Due to necking, the radius of curvature starts to increase until the forced elongation through the downward motion dominates and the curvature decreases again. After a certain period of time the bridge loses its constant curvature over the bridge height and is no longer considered in figure 10.

The three stages of the liquid bridge evolution during onset are illustrated in figure 9. In the first stage the pillar-shaped bridge is a consequence of the compression shown in i). The radius of curvature is smaller than the height, indicated through the larger diameter of the semicircles in figure 9 compared to the liquid bridge height. Therefore the liquid bridge radius of curvature does not match the proportionality of equation (1). Due to further stretching and simultaneous necking of the liquid bridge the radius of curvature increases up to ii) where $\kappa \approx 2/H$,

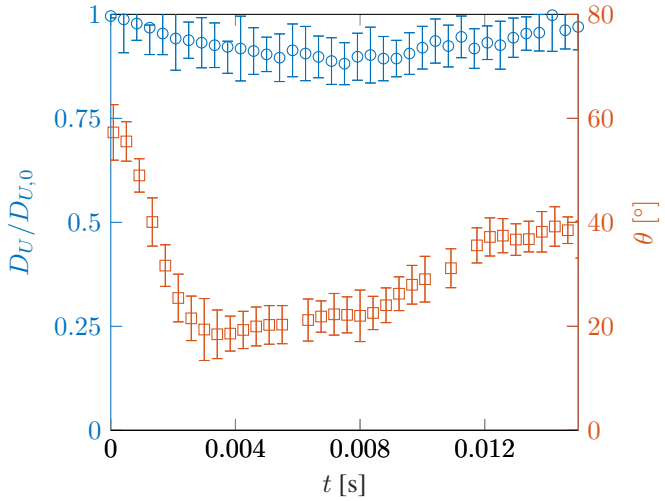

Figure 7. Comparison of the evolution of the contact line diameter $D_U/D_{U,0}$ with circle markers on the left scale vs. contact angle θ with square markers on the right scale. The experiments were performed with Gly80, $180\,\mathrm{m/s^2}$ and $k = 0.18$.

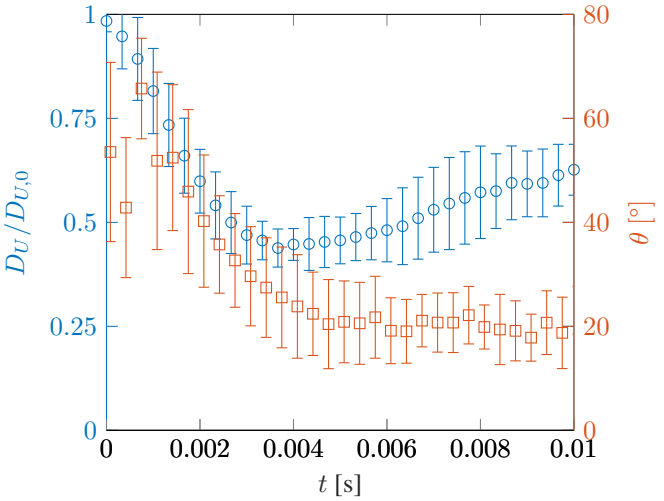

Figure 8. Comparison of the evolution of the contact line diameter $D_U/D_{U,0}$ with circle markers on the left scale vs. contact angle θ with square markers on the right scale. The experiments were performed with Gly80, $180\,\mathrm{m/s^2}$ and $k = 0.09$.

the half liquid bridge height is as large as the semicircles. During further stretching this proportionality remains valid until the necking no longer grows at the same rate as the bridge height. The radius of curvature begins deviating from the relation 1. The radius of curvature becomes smaller than the inverse height (1) shown in iii). The evolution with these three stages is better understandable with the data shown in figure 10. For different accelerations and viscosities the proportionality of the midpoint diameters and curvatures coincide.

$$\kappa = 2/H. \tag{1}$$

An approximation for the midpoint diameter evolution of the liquid bridge can be derived from the constant mass condition, see equation (2), comparing the volume of the liquid bridge with the evolution of D_M and H with respect their initial values $D_{M,0}$ and H_0. Depending on the dimensionless height parameter k the midpoint diameter deviates earlier for larger initial bridge geometries from the described proportionality. This relation is not limited by the constant curvature criteria and can be considered valid until break-up. All conducted measurements exhibit this behaviour for the first half of the shown evolution. This behaviour for different contact line diameters (k) indicates an independence between midpoint diameter and wetting behaviour.

$$D/D_{M,0} = \sqrt{H/H_0}. \tag{2}$$

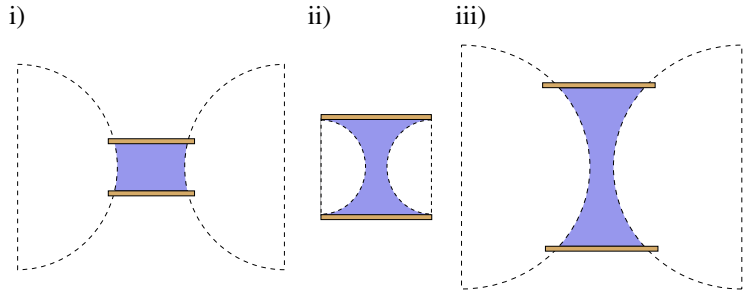

Figure 9. Evolution of the liquid bridge curvature during stretching. Showing a smaller curvature at the beginning in i) an increasing curvature due to necking in ii) and decreasing curvature as a result of the increasing vertical substrate distance in iii).

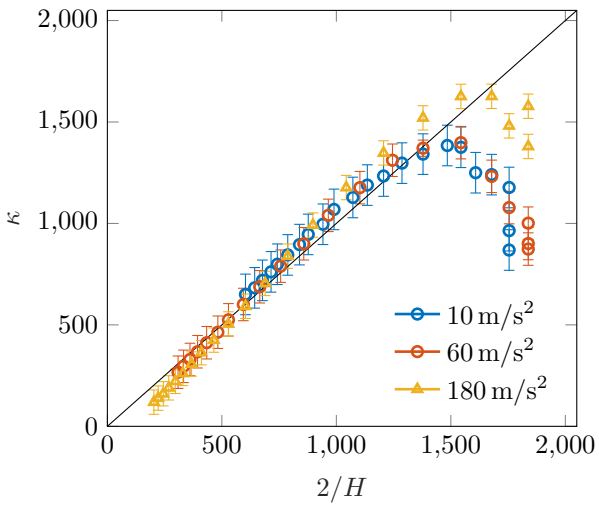

Figure 10. Evolution of the curvature and reciprocale height ratio for Gly80, $k = 0.3$ and different accelerations. The data points are from the constant curvature section.

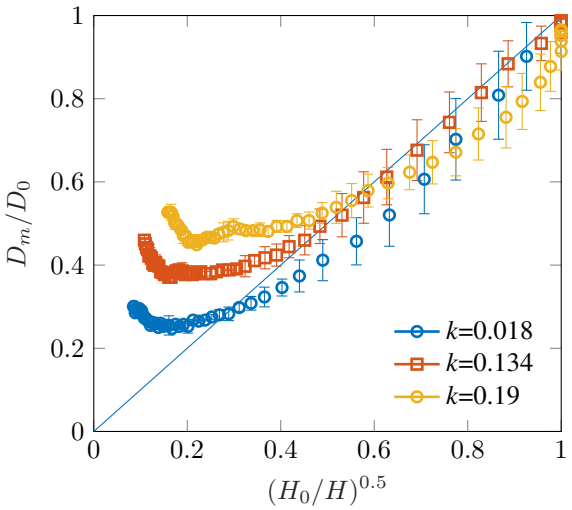

Figure 11. Evolution of the midpoint diameter and the inverse height derived from mass continuity, see equation 2. Measurements were performed with Gly80, 180 m/s^2 for different parameters of k.

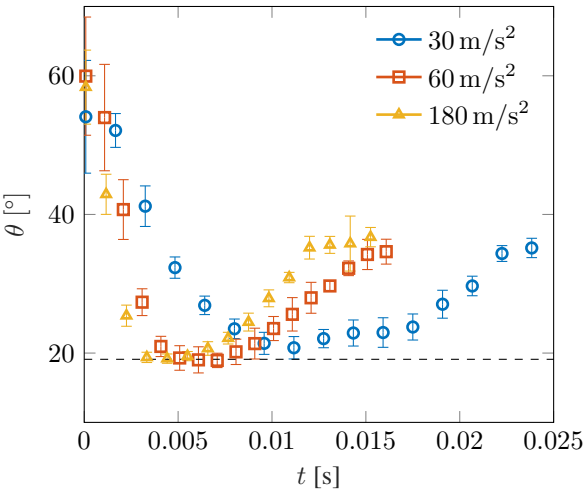

Figure 12. Evolution of contact angle of Gly80 comparing substrate accelerations 30, 60 and $180\,\mathrm{m/s^2}$ for $k = 0.3$. The dashed line indicates the measured receding contact angle.

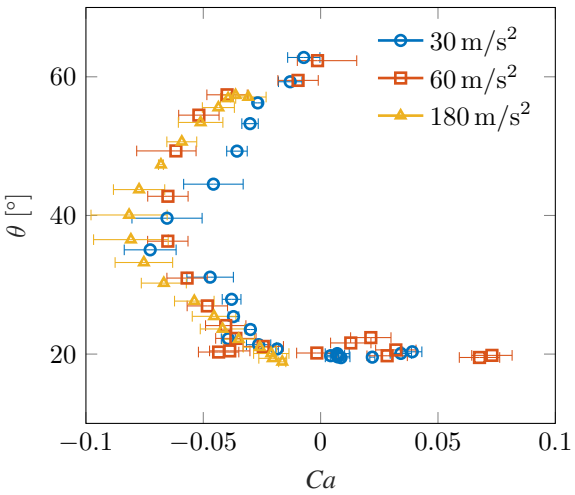

Figure 13. Evolution of the capillary number $Ca = U\mu\sigma^{-1}$ and the related contact angles. Measurements were performed with Gly80 and a dimensionless height $k = 0.1$

Since the contour of the liquid bridge can be assumed symmetric, a mean contact angle for both contact angles at the upper surface substrate θ_{up} is introduced. The contact angle evolution of θ is shown in figure 12 for Gly80, $k = 0.3$ and accelerations of 10, 60 and $180\,\mathrm{m/s^2}$. For all measurements the contact angle increases at the beginning due to the compressed state. The evolution of θ exhibits a steeper decline for higher accelerations until the curves reach a minimum $\theta_{\min}$. The minimum contact angle is of the order $\theta_{\min} = 19 \pm 1°$. This $\theta_{\min}$ agrees with the receding contact angle measured with a *KRÜSS DSA 100* system on the fluid/substrate combination. After the $\theta_{\min}$ is reached, the contact angle increases. The increase continues until shortly before the liquid bridge breaks at the meniscous region. The initial accuracy of the contact angle measurement is subjected to statistical errors due to optical resolution and the small initial bridge heights of $50\,\mu\mathrm{m}$.

The contact angle evolution is compared with the capillary number $Ca = U\mu\sigma^{-1}$ where U is the horizontal speed of the contact line in figure 13. The capillary number starts from the initial state $Ca = 0$ and decreases down to a contact angle of $\theta = 40°$. Depending on the acceleration, a minimum of $Ca \approx -0.09$ is reached for $180\,\mathrm{m/s^2}$. The contact line speed then starts to increase up to $Ca = 0$ and for some measurements even further. The contact angle does not drop below $\theta_{\min}$ as shown previously.

Summary and Conclusions

In this study the dynamic behaviour of contact angles and contact lines for different fluid properties, different initial bridge geometries and accelerations were analysed. The experimental setup allows investigation of fast liquid bridge stretching up to an acceleration of $180\,\mathrm{m/s^2}$.
The measurements demonstrate the relation between stretching acceleration and contact line movement. For the geometry of the liquid bridge, a proportionality for the early stretching process between the curvature and the inverse height was found. Furthermore a proportionality for the mid-point diameter evolution was developed. A strong effect of the initial bridge height on the contact line movement could be observed, showing that wettability effects have a greater impact on smaller liquid bridges. In future studies the dewetting process will be investigated further especially regarding different wettability states.

Acknowledgements

We kindly acknowledge the financial support by the German Research Foundation (DFG) within the Collaborative Research Centre 1194 "Interaction of Transport and Wetting Processes", Project A03.

References

[1] Weickgenannt, C., Roisman, I. V., and Tropea, C., *New Journal of Physics*, 17-8:083059 (2015).
[2] Villermaux, E., *Annual Review of Fluid Mechanics*, 39-1:419-446 (2007).

[3] Eggers, J., Villermaux, E., *Reports on Progress in Physics*, 71-3:036601 (2008).
[4] Dodds, S., Carvalho. M., and Kumar, S., *Physics of Fluids*, 23-9:092101 (2011).
[5] Dodds, S., Carvalho. M., and Kumar, S., *Journal of Fluid Mechanics*, 707:521-540 (2012).
[6] Chen, H., Tang, T., Zhao, H, Law, K.-Y., and Amirfazli, A., *Soft Matter*, 12-7:1998-2008 (2016).
[7] Roisman, I. V., *Physics of Fluids*, 16-9:3438-3449 (2004).